JOURNAL OF GEOPHYSICAL RESEARCH, VOL. 112, B03S02, doi:10.1029/2006JB004388, 2007

Click Here for Full Article

Coseismic fold scarps and their kinematic behavior in the 1999 Chi-Chi earthquake Taiwan

Yue-Gau Chen,[1] Kuang-Yin Lai,[1] Yuan-Hsi Lee,[2] John Suppe,[3] Wen-Shan Chen,[1] Yu-Nong N. Lin,[1] Yu Wang,[1] Jih-Hao Hung,[4] and Yu-Ting Kuo[1]

Received 14 March 2006; revised 29 July 2006; accepted 7 September 2006; published 13 March 2007.

[1] Discrete scarps that are created or reactivated during large earthquakes are a locus of concentrated hazard. A number of the coseismic scarps activated in the 1999 Chi-Chi earthquake are actually fold scarps, which display several types of ground deformation characterized by localized folding and are distinct from classic fault scarps, which form by a fault cutting the surface. This paper documents and analyzes fold scarps that formed or reactivated in the 1999 Chi-Chi Taiwan earthquake. Our results show the Chi-Chi fold scarps can be generally divided into two types: (1) those associated with folding ahead of the tip of a blind thrust fault at shallow depths and (2) those associated with folding by kink band migration above fault bends at substantial depths ranging from ~0.8 to 5 km). The previously published trishear model can be applied to model the former type, while a new curved hinge kink band migration model is provided to describe the behavior of the latter type. A key feature of fold scarps of the second type is that hinge zones are typically wide (25–100 m) relative to the displacement in a single earthquake (1–10 m), which exerts a significant control on fold scarp morphology and evolution. Because the coseismic strains of both types of fold scarps display relatively wide deformation zones (10–100 m) relative to fault scarps, wider set-back zones might be appropriate from a public policy point of view to alleviate the risk to structural damage and collapse resulting from permanent ground deformation.

Citation: Chen, Y.-G., K.-Y. Lai, Y.-H. Lee, J. Suppe, W.-S. Chen, Y.-N. N. Lin, Y. Wang, J.-H. Hung, and Y.-T. Kuo (2007), Coseismic fold scarps and their kinematic behavior in the 1999 Chi-Chi earthquake Taiwan, *J. Geophys. Res.*, *112*, B03S02, doi:10.1029/2006JB004388.

1. Introduction

[2] Taiwan is located on the continental shelf of south China at the boundary between the Eurasia and Philippine Sea plates (Figure 1a) where an arc-continent collision has been operating since the early Pliocene, producing the west vergent fold-and-thrust belt in western Taiwan [*Ho*, 1982; *Suppe*, 1986; *Teng*, 1990]. Because the collision is ongoing, large earthquakes occasionally happen with significant damage and loss of life. In the last century the largest event was the 1999 Chi-Chi earthquake M_w 7.6, which resulted in over 100,000 severely damaged buildings and 2400 fatalities. A major source of reported damage and loss of life was concentrated where the larger surface deformations occurred; especially the surface rupture scarps, which are distributed over a distance of 100 km from south to north [*Central Geological Survey* (*CGS*), 1999] (Figure 1b). The most important seismogenic fault of the composite Chi-Chi earthquake is the Chelungpu fault, which is the second thrust fault eastward from the western deformation front [*Chiu*, 1971; *Chinese Petroleum Company*, 1982; *Suppe*, 1981; *Yue et al.*, 2005] (AA′ in Figure 2). Most of the coseismic Chi-Chi scarps formed where the main fault reached the surface [*CGS*, 1999; *Chen et al.*, 2002]. Nevertheless, postearthquake investigations demonstrate that some of the coseismic scarps are characterized by wider zones of bending without an associated major fault cutting the land surface, in contrast with typical fault scarps. These are actually fold scarps [*Suppe et al.*, 1997; *Dolan et al.*, 2003; *Hubert-Ferrari et al.*, 2007] based on the evidence presented in previous and present study [*Chen et al.*, 2004; *Lee et al.*, 2005; *Lai et al.*, 2006]. Here we discuss the types, mechanisms, and coseismic behavior of folds scarps based on the observations of the coseismic examples of the 1999 Chi-Chi earthquake.

[3] It is common to misidentify fold scarps as fault scarps because the geomorphic profile of a monoclinal, kink shaped fold scarps can superficially resemble fault scarps where the overhanging hanging wall has collapsed during or shortly after an earthquake, as well those that have under-

[1]Department of Geosciences, National Taiwan University, Taipei, Taiwan.
[2]Department of Earth and Environmental Sciences, National Chung-Cheng University, Chiayi, Taiwan.
[3]Department of Geosciences, Princeton University, Princeton, New Jersey, USA.
[4]Department of Earth Sciences, National Central University, Chungli, Taiwan.

Copyright 2007 by the American Geophysical Union.
0148-0227/07/2006JB004388$09.00

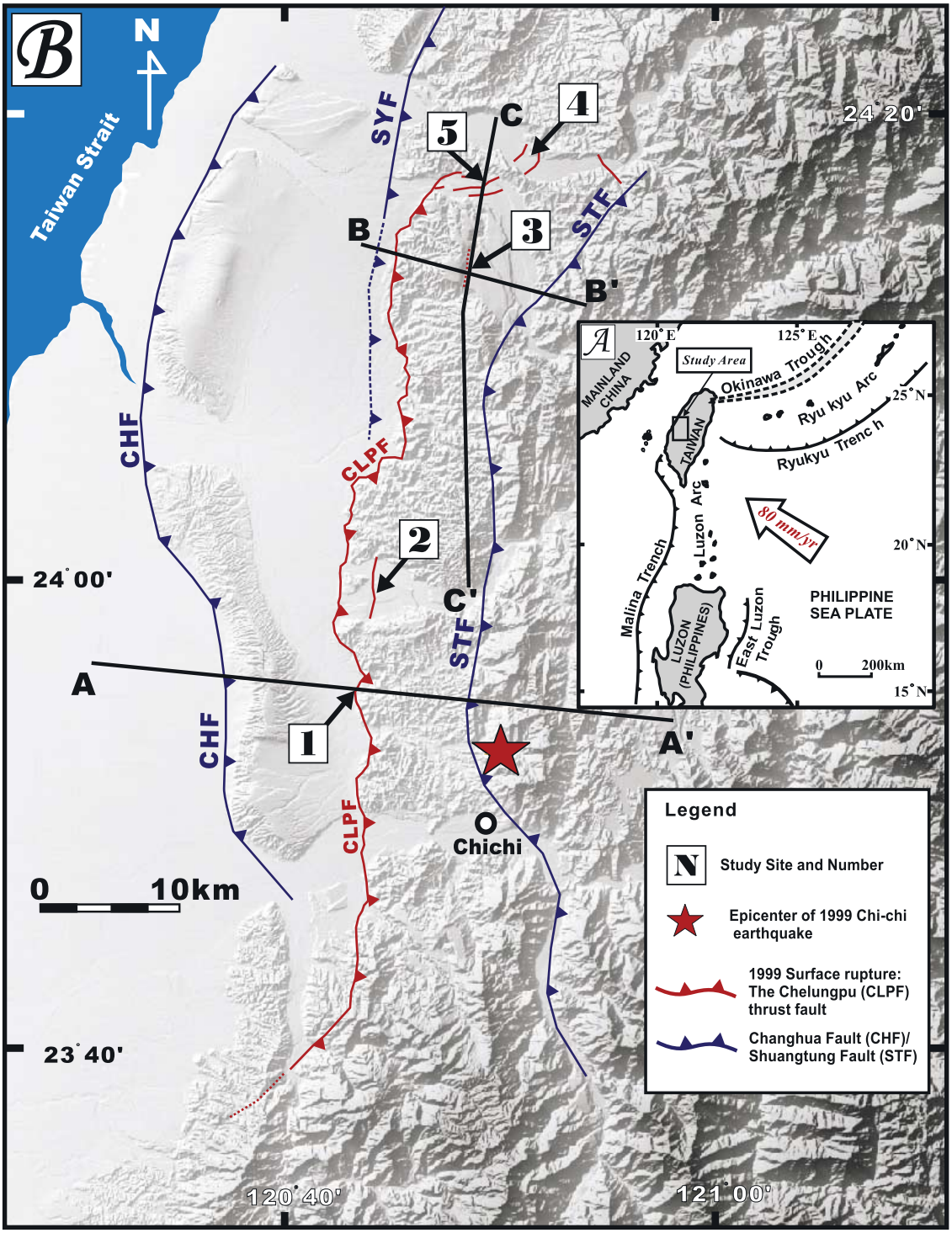

Figure 1. (a) Current tectonic environment surrounding Taiwan and study area. Velocity for the plate motion is adopted from *Yu et al.* [1999]. (b) Map showing the topography in central Taiwan and study sites. Major thrust faults are shown, such as CLPF, Chelungpu fault (1999 surface rupture); STF, Shuangtung fault; SYF, Sanyi fault; CHF, Changhua fault. Note that site 1 is Shijia trenching site, Nantou; site 2 is Tsaotun; site 3 is Hsinshe; site 4 is Neiwan; and site 5 is Hsiaolipu.

gone long-term erosion [e.g., *Yielding et al.*, 1981]. As a result, more than the correct number of active faults will be defined on geological or seismic hazard maps. Also, the setback zone designated for fold scarps above fault bends as well as for fold scarps above blind faults will be also inappropriate since the coseismic surface deformation for a fold scarp is quite different from a fault scarp. The 1999 Chi-Chi event provides an important opportunity to quantitatively document the differences between these two superficially similar but fundamentally different fault-related zones of localized coseismic deformation. For the purpose of understanding the mechanism and coseismic

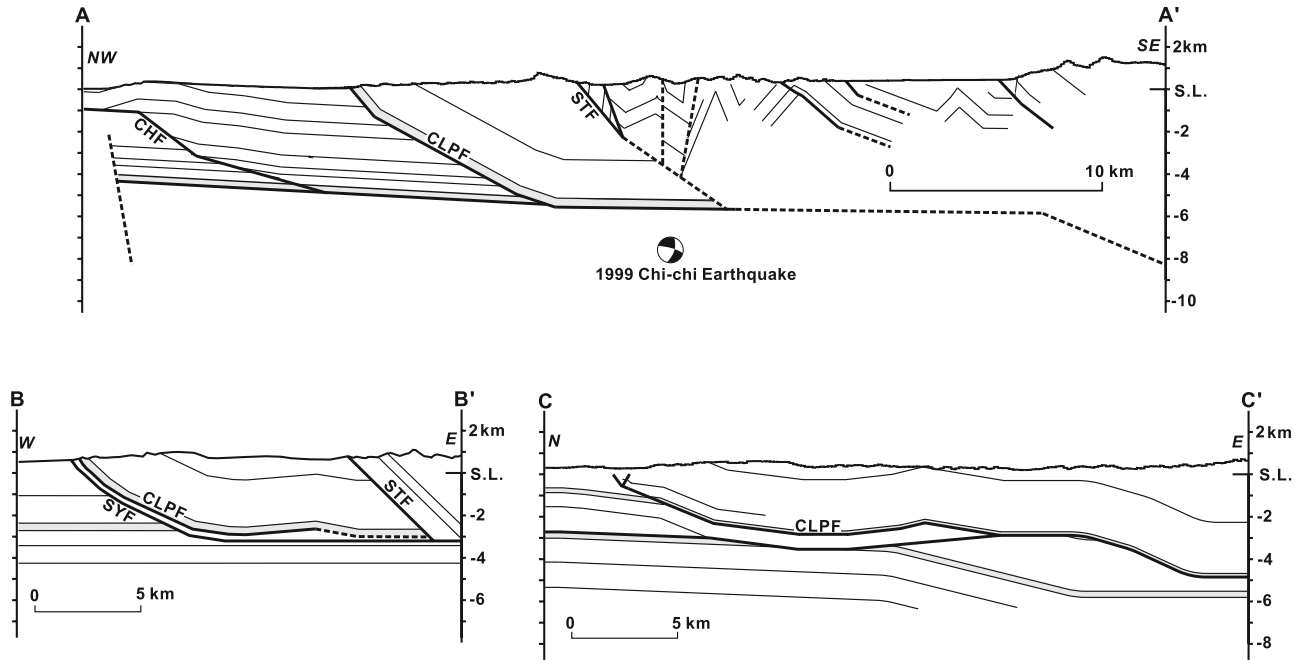

Figure 2. Cross sections showing the subsurface geology in the hanging wall of the Chelungpu fault (line index map in Figure 1b). Please note the bends in the fault plane of the Chelungpu fault at depths of 2 km, 3 km, and <1 km in (a) AA′, (b) BB″, and (c) CC′, respectively, discussed in the text.

behavior of these active scarps, we made field measurements of the surface deformation as well as the subsurface structures. In addition we present a simple kinematic model of one of the two types of fold scarps to help explain the coseismic deformation that we observed in 1999 event. To completely establish the behavior of these scarps, further studies of subtle geomorphic features and their age determination are still needed.

2. Fault Scarps and Fold Scarps Formed in the Chi-Chi Earthquake

[4] Because of the shallow source and large slip reaching 3–10 m in the 1999 event [*CGS*, 1999; *Ma et al.*, 1999; *Kao and Chen*, 2000], the main thrust commonly reached the ground surface and formed a fault scarp over much of its ~100 km length. Typical thrust fault scarps found in the 1999 event are characterized by substantial horizontal shortening and loss of surface area, which is absorbed in a narrow zone along the fault trace regardless of whether it is the main fault or a subsidiary fault. This loss of surface area results in a footwall buried by up to 10 m of the hanging wall. In contrast with these typical thrust fault scarps, fold scarps are also found but are characterized by a wider surface deformation zone reaching 25–100 m and essentially no loss of surface area. The fold scarps found in the 1999 event can be divided into two types (type 1 and type 2 in the following text) based on the mechanisms of formation, as follows.

3. Coseismic Deformation of Fold Scarp Associated With a Blind Thrust Tip: Type 1 Site 1 Shijia Trenching Site in Nantou

[5] Type 1 fold scarps are closely related to fault scarps because they are created as a result of burial of an active fault trace by thick deposition in the interseismic period. The fold scarp forms by distributed coseismic deformation ahead of the fault tip within the previously undeformed surficial strata deposited since the last earthquake. To illustrate the type 1 fold scarps, we describe a well-studied case located in the southern segment of the Chelungpu fault (site 1 in Figure 1). This is a trench site with supporting shallow boreholes, which is originally named as Shijia (i.e., the Chinese fruit name, also known as Buddha head) because this fruit grew on the ground surface before the earthquake. The postearthquake investigation of the scarp, based on the regular structure of the fruit field, showed that it is a fold scarp because there was no associated loss of surface area of the sort that would be expected if this were a fault scarp with a buried footwall. A trenching study was conducted for the purpose of paleoseismology [*Chen et al.*, 2004; *Streig et al.*, 2006] (Figure 3a). The trench log shows continuous sedimentary layers underlying the topographic scarp, indicating the fault tip stops at least 5m below the surface, which is the depth of the trench. The fault tip can be further constrained to lie at 5–10 m in depth because the borehole C2 drilled through the fault (Figure 3a). In this case, the surface scarp is definitely not a typical fault scarp, which is consistent with the observation of no fault disruption on the surface. Judging from the differential uplift across the scarp, the surface deformation can be described as a scarp created by folding behavior. The trenching study [*Streig et al.*, 2006] applied the concept of fault tip migration and trishear folding to model the coseismic deformation [*Erslev*, 1991; *Hardy and Ford*, 1997; *Champion et al.*, 2001] (Figure 3b). Fault dip and tip position is constrained by boreholes C1 and C2. The deformed layer shapes are the basis for inverse modeling of the slip and best fitting fault geometry. Using the parameters of the best fit model, a forward model is constructed and presented in Figure 3b.

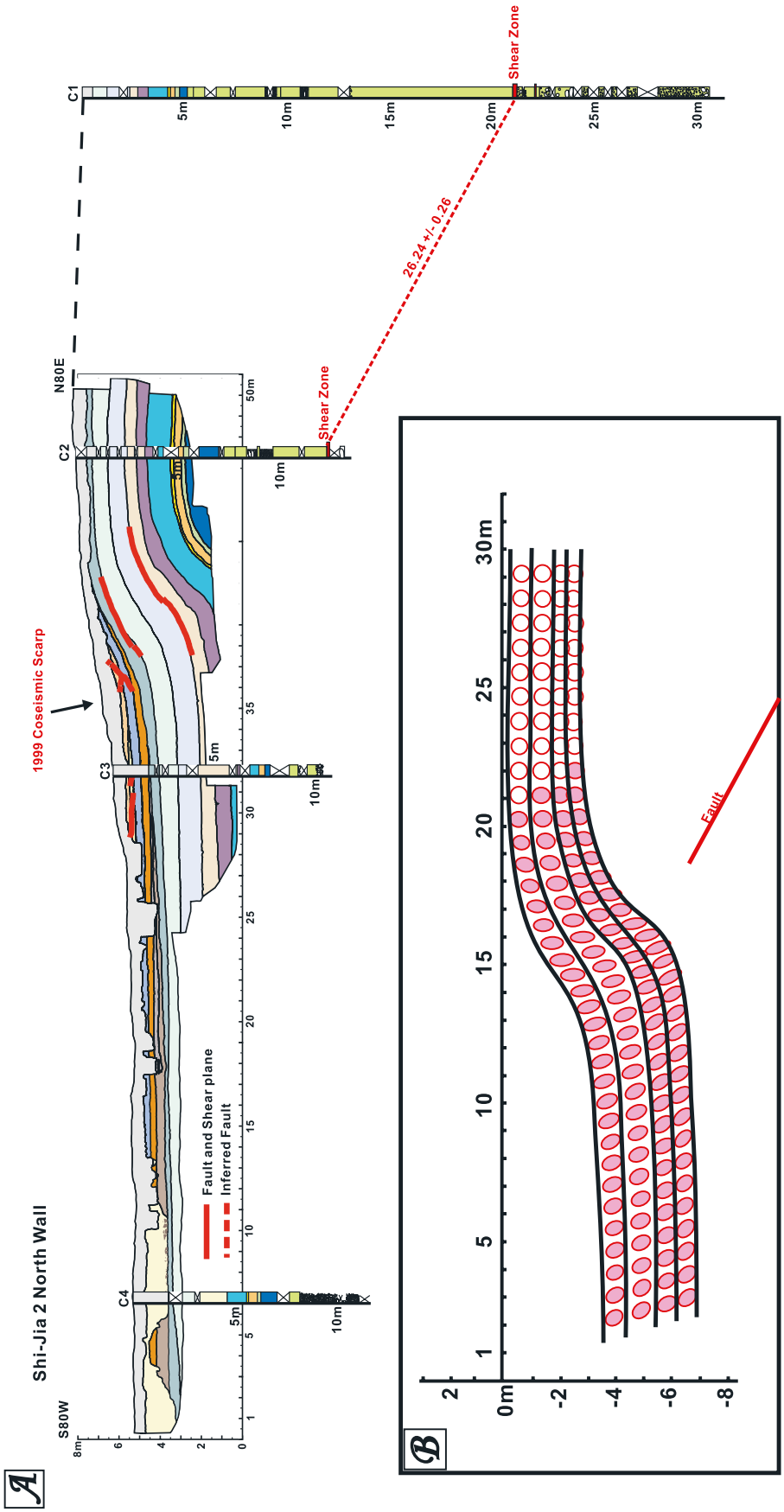

Figure 3. (a) Profile illustrating logs of the trench site Shijia at Nantou and four supporting boreholes C1 to C4 [*Chen et al.*, 2004; *Streig et al.*, 2006]. The surface scarp of the 1999 Chi-Chi earthquake lies between C2 and C3. From the fault zone identified in C1 and C2, the Chelungpu fault can be inferred to have a dip angle of 26°E and a position in the depth range of 10 to 20 m. The fault tip is constrained to be in the depth range of 5 to 10 m between C2 and C3. (b) Modeled result showing the strain distribution across the fold scarp. Note that significant surface shortening occurs from the top of the scarp to at least 10 m beyond the scarp toe.

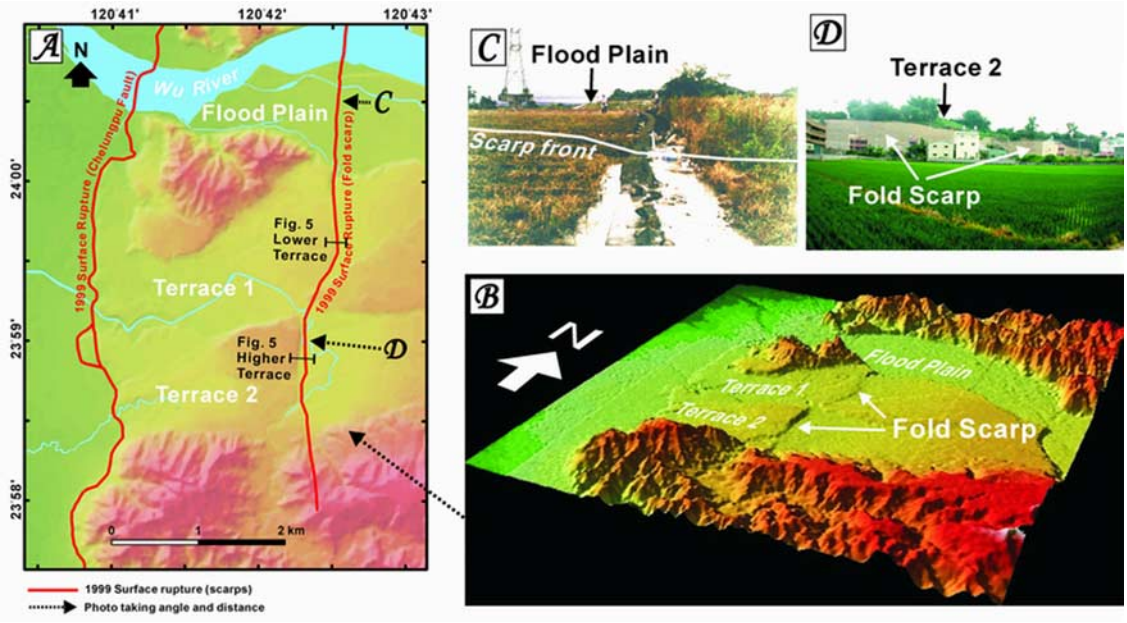

Figure 4. (a) Shaded relief map of Tsaotun area showing the 1999 surface deformations, which are composed of two major scarps: the west facing main fault scarp in the west and an east facing fold scarp in the east. (b) The 3-D DEM model viewed from the southeastern showing two major terrace sets (terrace 1 and 2 in the Figure 5) and the modern floodplain of the Wu river. (c) Photo taken facing the fold scarp created during 1999 Chi-Chi earthquake. Please note the retaining wall of the corn field is folded but no significant shortening observed. (d) Overview photo taken facing the fold scarp across the old terrace 2. Most of the buildings that survived were located away from the scarp, while those constructed on the scarp were all tilted by the coseismic surface deformation and destroyed.

The result shows significant strain distributed from the top of the scarp to 10 m beyond the scarp toe, which is entirely different from what is observed in thrust fault scarps. The shortening given by thrust faulting is largely absorbed by layer thickening due to the ductility of the covering unconsolidated sediments. Substantial layer thickening occurs across the scarp. According to this trishear modeling result, the scarp shape is controlled by the fault dip, the position of the fault tip, and the amount of slip. If the geologic parameters mentioned above were all known before the earthquake, the coseismic deformation of the fold scarp could actually be predicted.

4. Coseismic Deformation of Fold Scarp Associated With Fault Bend: Type 2

[6] Type 2 fold scarps of the Chi-Chi earthquake are typically found in the hanging wall far removed (>km) from the surface trace of the associated fault, in contrast with type 1 fold scarps which are closely associated with the fault tip and located within the general zone of the surface fault trace. Type 2 fold scarps are directly associated with abrupt dip changes in the fault at depth and with dip changes in the hanging wall bedding. This paper presents data from four sites (sites 2 to 5 in Figure 1b): Tsaotun, Hsinshe, Neiwan, and Hsiaolipu. The first two sites, Tsaotun and Hsinshe, are located several kilometers to the east of the Chelungpu fault surface trace and had a linear preexisting east facing topographic scarp (Figures 2a and 2b), which had been previously interpreted as a fault scarp formed by mountain-ward back thrusts [*Ku*, 1963; *Bonilla*, 1977; *Shih et al.*, 1985, 1986]. However, during the 1999 event the coseismic surface deformation surprisingly demonstrated folding behavior instead of faulting, indicating the scarps are actually fold scarps generated by differential slip in response to fault bends at depth. The final two sites, Neiwan, and Hsiaolipu, are within the northern complex ~1–2 km wide zone of complex Chi-Chi surface scarps which strikes due east to NNE. This zone at Neiwan and Hsiaolipu is actually the preexisting Tungshih anticline which grew coseismically by ~10 m resulting from consuming the slip at the termination of the Chelungpu fault at depth (Figure 2c).

5. Site 2 Tsaotun: A Preexisting Fold Scarp

[7] This fold scarp found ~2 km to the east of the main surface trace of the Chelungpu fault (Figure 4) was a preexisting scarp and regarded as a fault scarp before 1999 (namely, the Ailiaochiao fault [*Shih et al.*, 1985], Figures 4a and 4b). There are three major river terraces (Figure 4) including a higher terrace (terrace 2 in Figure 5), lower terrace (terrace 1 in Figure 5), and a recent floodplain (Figure 4c). Before 1999, two older geomorphic surfaces had been displaced by this fold scarp, but the recent floodplain had not yet been affected (Figures 4b and 4c). Field investigation demonstrates that the coseismic surface deformation is a wide tilting instead of a clear fault scarp. Furthermore, reconnaissance along the bank of the Wu River found no evidence indicating a fault but only an abrupt change in the dip of underlying bedding across the scarp trace (Figure 5). The measured bedrock dips in the

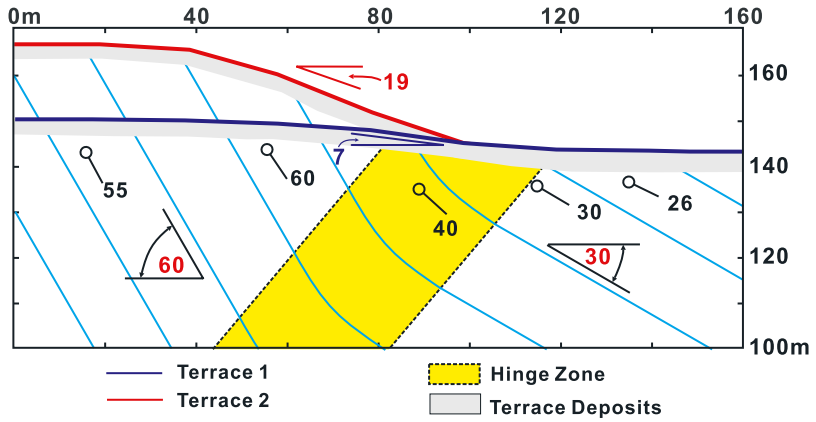

Figure 5. Fold scarp profiles east of Tsaotun showing the reconstructed subsurface structure across the fold scarp. Also shown on the top is the projected topography of the old and young terraces (see Figure 4a for locations). The older terrace underwent a relatively long history of deformation on the Chelungpu fault and has already reached the maximum slope angle (19°, please see text for details), whereas the young terrace has not yet reached this value.

west and east are 58–60°E and 30–32°E, respectively. The width of the hinge zone of changing dip is estimated to be 40 m in horizontal distance. Since the Chelungpu fault has evolved as a bedding parallel thrust fault, the dip change can be interpreted as a fault bend at depth (AA′ in Figure 2). A two-dimensional schematic model is presented in Figure 6 to illustrate the kinematics of the fault movement and associated fold scarp development.

5.1. Model of a Fold Scarp Created by a Fault Bend

[8] We develop a simple model of fold scarp formation above a fault bend to help explain the type 2 mechanism of fold scarp formation. In Figure 6, the thrust fault consists of three elements: the shallow high-angle (θ_2) segment, the deep low-angle (θ_1) segment, and a zone of finite width over which the fault dip changes monotonically. The hanging wall of the main thrust fault can therefore be divided into three corresponding components: θ_2 domain, θ_1 domain, and hinge zone area. The hinge zone is geometrically like a tilted synclinal axial surface that bisects the fold thereby conserving layer thickness. Overlying the entire structure before the next increment of deformation is a horizontal reference surface that might correspond to an undeformed terrace, road, etc. In the case of Tsaotun, the initial reference surface is a river terrace developed by river incision. To simplify the model, we assume this initial reference surface is flat in the beginning. The slip occurs along the fault plane, parallel to the bedding planes. Other than the fault plane no other discontinuity is allowed. Any dilatancy associated with the fault bend is ignored as second order. As the fault slips episodically event by event, the particles initially positioned in the θ_1 domain will move horizontally by the event slip multiplied by $\cos(\theta_1)$ and will move vertically by the slip multiplied by $\sin(\theta_1)$. Upon reaching the hinge zone the vertical component increases, while the horizontal component decreases. As slip accumulates through successive earthquakes, these particles will move through the hinge zone and arrive in the θ_2 domain, where the particles undergo displacement increments equal to the event slip times $\cos(\theta_2)$ and $\sin(\theta_2)$ for the horizontal and vertical components, respectively. Because $\sin(\theta_2) > \sin(\theta_1)$ the original terrace will not remain flat after the first slip event. Obviously all particles initially located in zone θ_2 above and west of the hinge zone will all have the same cumulative vertical displacements, therefore this part of surface will remain flat (Figures 6b, 6c, and 6d). Each particle originally located within the hinge zone (segment $\mathbf{a_0}$) will undergo different cumulative vertical displacements, which decrease eastward in response to the smaller vertical component to the east. Therefore an east dipping slope will form and become steeper as slip accumulates with time. Once all the particles originally located within the hinge zone reach the θ_2 domain, the slope angle will reach a maximum (ϕ in Figure 6c) because all the particles entering the θ_2 domain are now from the θ_1 domain and will have traversed the entire hinge zone. From that time on, the width of the scarp will keep growing as the fault continues slipping, but the scarp slope angle will stop growing and remain at ϕ. In contrast, the scarp height (Figures 6b, 6c, 6d, and 7) will continue to increase as time advances, but the surface erosion will eventually limit the height of the scarp. The final scarp shape reflects the cumulative difference in displacement among the particles initially positioned on the terrace surface. As described in Figure 7, the surface of a type 2 fold scarp eventually consists of three components: two zones of changing slope (a and c in Figure 7) at the top and bottom of the scarp and a maximum slope (b in Figure 7) in between. The lengths of two zones of changing slope are equal and identical to the arc length of the dip change zone.

5.2. Maximum Slope Angle ϕ

[9] For a type 2 fold scarp, how do we know whether or not the maximum slope has been reached? In this study, we further use the concept of similar figures and trigonometric function to obtain the relationship (Equation 1 and Appendix A) between maximum slope angle ϕ and the bedding dips (θ_2 and θ_1):

$$\tan(\theta_2 - \phi) = \frac{\sin\theta_1 \cos\left(\frac{\theta_2-\theta_1}{2}\right)}{\cos\left(\frac{\theta_2+\theta_1}{2}\right) - \sin\theta_1 \sin\left(\frac{\theta_2-\theta_1}{2}\right)}. \quad (1)$$

Since θ_2 and θ_1 are both measurable in the field, the maximum slope angle ϕ can be computed and compared

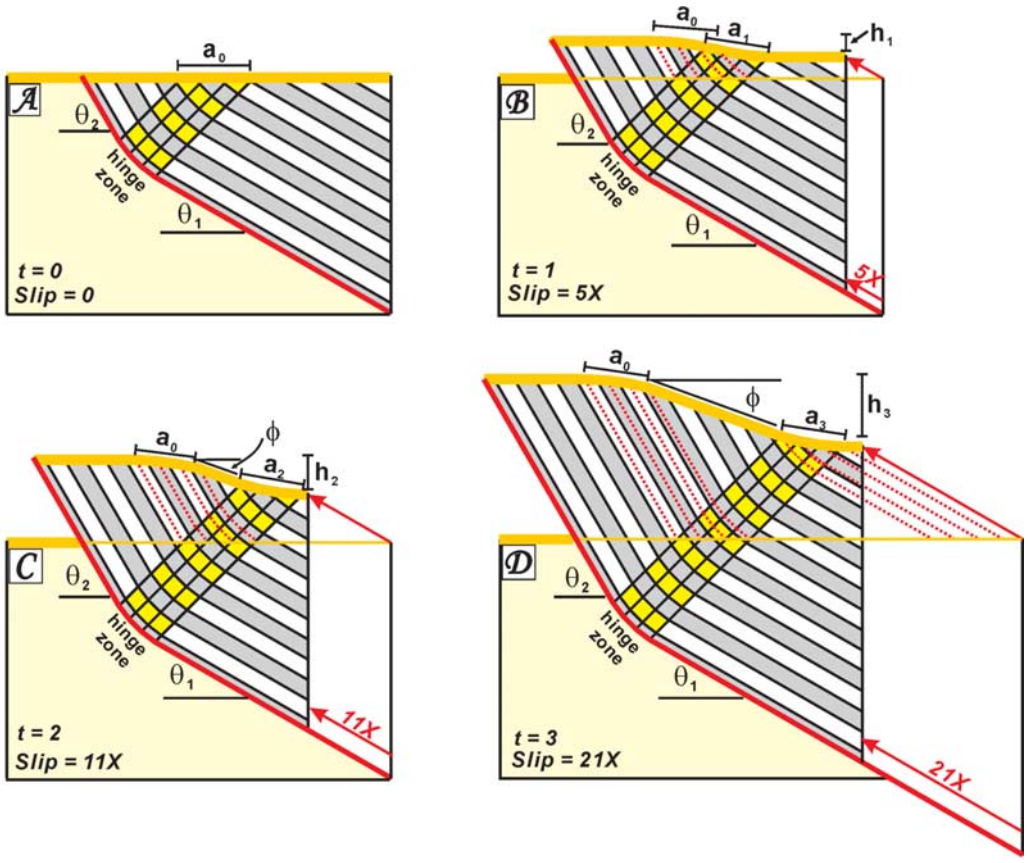

Figure 6. Schematic kinematic model of fold scarp development in the case of Tsaotun, where θ_1 and θ_2 are 30° and 60°, respectively. A fault bend is assumed at an arbitrary depth and the hinge zone is marked in yellow. To model the kinematic behavior, the event slip is given as X, which is small relative to the hinge zone width and is constant along the length of the fault plane. (a) Geomorphic surface forms by erosion after earlier deformation and is assumed to be initially flat. The particles lying within the initial surface projection of the hinge zone are noted as $\mathbf{a_0}$. (b) After five events the fold scarp becomes rather clear. The initial $\mathbf{a_0}$ is still partially within the active hinge zone area. (c) After 11 events, $\mathbf{a_0}$ has been moved away from the active hinge zone. A topographic segment with the maximum fold scarp dip (ϕ) appears between $\mathbf{a_0}$ and active hinge zone (see Appendix A for the deduction). (d) Fold scarp keeps growing, and the topographic segment of maximum dip extends in length but the angle remains the same. The scarp height increases linearly event by event but is always equal to that event slip times [$\sin(\theta_2) - \sin(\theta_1)$].

with the current slope angle. For the case of Tsaotun, the bedding dips, θ_1 and θ_2, are 30° and 58°, respectively. On the basis of the relationship presented above, the maximum slope angle ϕ will be 19°. Checking the scarp profiles for higher and lower terrace (terraces 2 and 1 in Figure 5), it is evident that the higher terrace has experienced a long history of fault action and the maximum slope angle has been reached. On the other hand, the lower terrace only has an angle of 7°, implying it is still in the beginning stage of the scarp development. For the practical use in the field, we further compute the maximum slope angle ϕ for other possible cases, as shown in Figure 8, in which the abscissa is smaller dip θ_1 and each curve denotes the solution for a constant change in dip ($\theta_2 - \theta_1$).

6. Site 3 Hsinshe: Another Preexisting Fold Scarp

[10] The Hsinshe site is a major preexisting fold scarp, located in the hanging wall of the northern segment of the

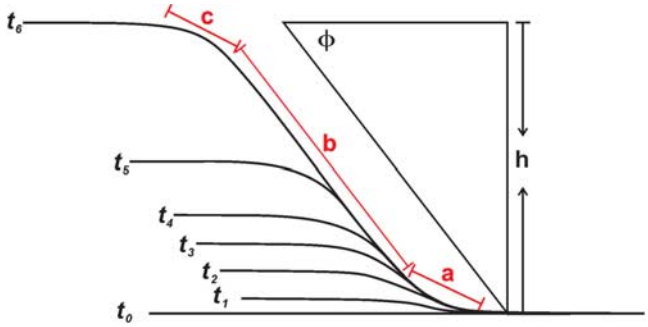

Figure 7. Successive evolution of fold scarp shapes illustrated for arbitrary times t_0 to t_6. From the moment the maximum slope ϕ angle appears the scarp consists of three elements: "a", "b", and "c". The widths of "a" and "c" are identical and same as the arc length as the hinge zone. The length of "b" grows as the fault continues to accumulate displacement and the height "h" of the scarp continuously increases.

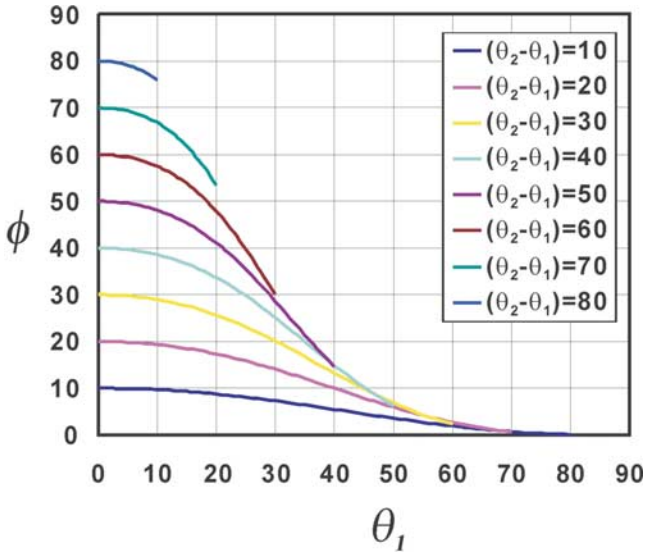

Figure 8. Diagram illustrating the relationship between ϕ, θ_1, and θ_2 (see Appendix A). From observed values of fault dip θ_1 and constant values of change in fault dip ($\theta_2 - \theta_1$), represented by the color curves, the maximum slope angle ϕ of the fold scarp can be suggested for any specific case.

Chelungpu fault, 6 km to the east of the surface fault trace. This scarp had previously been interpreted as a fault scarp (Figure 9a) [*Shih et al.*, 1986] but the underlying bedrock geology shows it to be a fold [*Yue et al.*, 2005; *Lai et al.*, 2006]. Furthermore the scarp shape is distinctly different from nearby terrace risers because of its relatively gentle slope (18°) with a kink-shaped profile as expected for a fold scarp as opposed to a degraded terrace riser or fault scarp (Figure 9b). Post-Chi-Chi investigations show it to be a fold scarp based on the 1999 coseismic ground displacement mainly measured by GPS and on the structure reconstruction made from field measurements [*Lai et al.*, 2006] (BB′ in Figure 2). The configuration at Hsinshe resembles the case at Tsaotun. There is an associated fault bend along the Chelungpu fault at a depth of 4 km with the hanging wall bedding parallel to the fault plane. The bedding dip below the folded terrace changes from 5°E to 23°E across the fold scarp going from east to west (Figure 10). The hinge zone cannot be clearly recognized in the field because of the discontinuous exposures; however, it still can be estimated to be ~150 m wide. According to the discussion above (Figure 8), the θ_1 and θ_2 are 5° and 23°, respectively, and the maximum slope angle ϕ is 18°, identical to the current slope angle. This result reveals the cumulative fold scarp at Hsinshe has evolved into a mature state.

7. Site 4 Neiwan and Site 5 Hsiaolipu: Fold Scarps Associated With a Fault Bend Fold

[11] At the northern end of the Chelungpu fault, the zone of localized 1999 Chi-Chi surface deformation bends eastward and becomes two parallel sets of surface monoclinal kink folds (i.e., the short limb is a few meters in scale), which are the focus of our sites 4 and 5 (Figure 11a). These kink folds were mistaken as fault scarps but redefined as fold scarps after recognition of the deformation behavior in the 1999 event, which is characterized by a preservation of surface area (Figures 11b to 11f). Most of the outcrops show no fault at the surface and the deformation is characterized by tilting along the scarp zone. A previous study [*Lee et al.*, 2005] presented a geodetic transect across the recent floodplain at Neiwan and showed an anticlinal shape of the surface warping. The coseismic scarp distribution and locus of Chi-Chi uplift match with the previously known Tungshih anticline in the bedrock [*Hu and Chiu*, 1984], indicating it is still active and coseismically grew by 10 m during the 1999 earthquake [*Lee et al.*, 2005] (Figure 12c). Kinematically it is a fault bend fold created by the updip termination of the Chelungpu fault into the shallow crust (CC′ in Figure 2). The fold scarps are developed in terraces and coincide with abrupt change in bedrock dip (Figures 11e, 12, and 13) similar to the Tsaotun and Hsinshe cases presented above.

7.1. Neiwan Profile

[12] At Neiwan a structural profile is established by continuous bedding measurements below the strath of the recent floodplain, which is tied to the surface profile of the terrace overlying the strath and presented in Figure 12a. Since the recent floodplain had no scarp before the earthquake and the river was graded as shown by pre-1999 river profiles created from the 40 m Taiwan DEM, the topographical anomalies illustrated in Figure 12 can be regarded as the coseismic deformation as shown by *Lee et al.* [2005]. The Tungshih anticline in this area has a near-surface width of 1 km, showing a flat top and two tilted limbs. Both limbs have sharp anticlinal hinges which were not activated in the Chi-Chi earthquake; instead the fold scarps are associated with synclinal bends at the base of the fold limbs (Figures 11a to 11f and 12a to 12c). The coseismic activation of just one hinge of each fold limb (the synclinal hinges in these cases) is consistent with the kink band migration mechanism of fold scarp formation (see Figure 6) as opposed to fixed hinge limb rotation mechanisms. The western limb shows a relatively gradual dip change over a surface distance of more than 40 m, generating a long wavelength and gentle fold scarp (Figure 12b). In contrast, in the eastern limb, the dips change over in a relatively short distance of only 10 m (Figure 12c). During 1999 event, a fold scarp formed that is steeper than its western counterpart. Unfortunately this eastern scarp passes through a populated town and caused severe damage and casualties (Figures 11b, 11c, and 11d). Considering the maximum slope angle discussed above, the (θ_1, θ_2) for both of the western and eastern limbs are (23°, 40°) and (3°, 32°), respectively. The corresponding maximum slope angles are 14° and 29°. The measured slope angles of the fold scarps are 8° and 20°, both less than the corresponding maximum value. This implies the slope angle will grow in future earthquakes.

7.2. Hsiaolipu Preexisting Scarp

[13] At Hsiaolipu (site 5) we reexamine the 40 m Taiwan DEM produced before 1999 and find the rupture scarp is actually a preexisting one; however, none of the previous literature reported this scarp. During the 1999 Chi-Chi earthquake it reactivated and caused minor damage because it runs mainly through the fruit fields (Figure 11c). The outcrop exposed along the river bank (Figure 11e) demonstrates the strata underneath the scarp are all continuous but

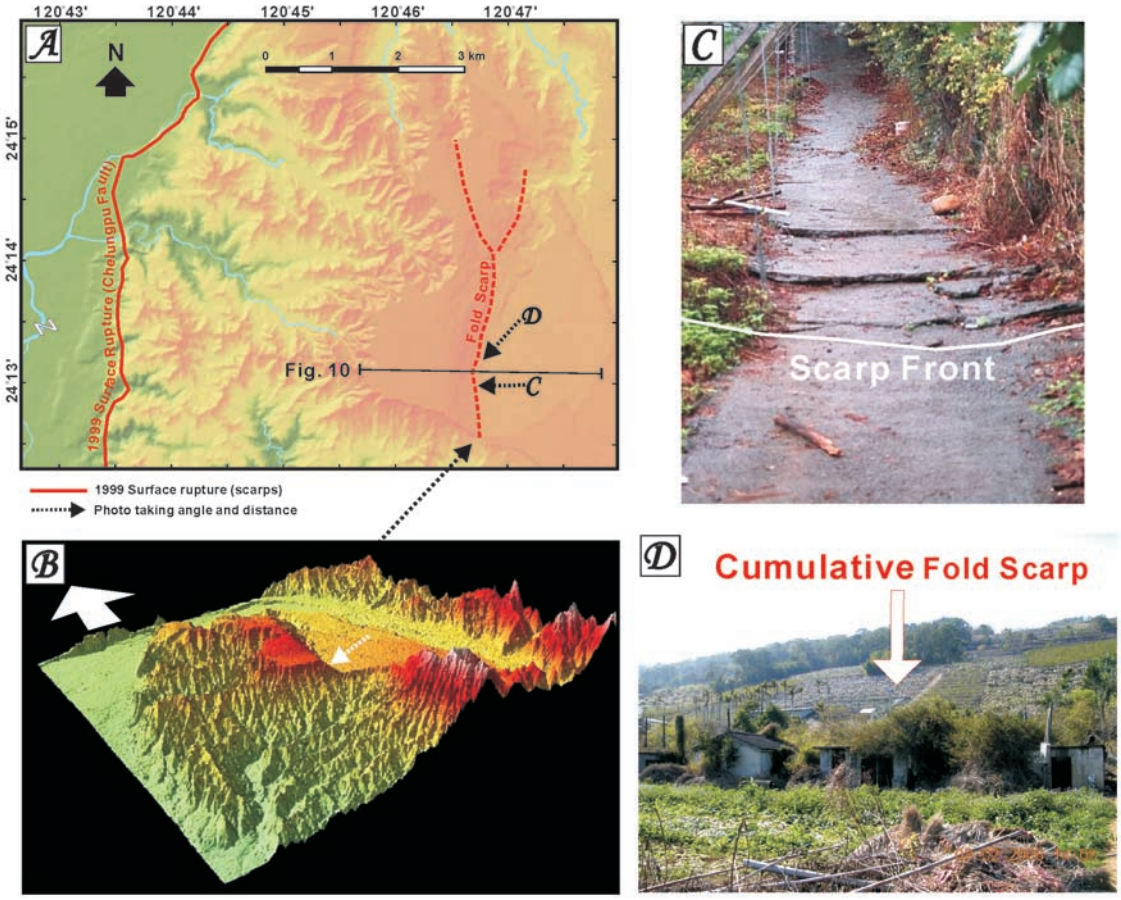

Figure 9. (a) Shaded relief map of Hsinshe area showing that the structural setting east of the Chelungpu surface break is similar to Tsaotun (Figure 4) where the 1999 surface ruptures consisted of two major scarps: the west facing main fault in the west and an east facing fold scarp in the east. (b) The 3-D DEM model viewed from the southwestern, showing the kink shape of the cumulative fold scarp on the old terrace (white arrow in the middle). (c) Photo showing the scarp toe with minor compressional faulting that formed during the 1999 earthquake. (d) Photo showing the 18° dipping surface of the cumulative fold scarp, which corresponds to the "b" segment in our model (Figure 7).

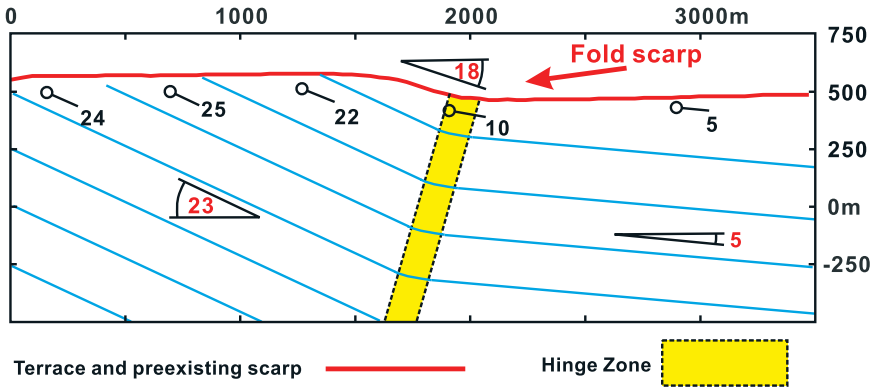

Figure 10. Regional profile of the Hsinshe cumulative fold scarp and its related subsurface structure, which is reconstructed based on field measurements of bedding and data from the published geological map [*Chinese Petroleum Corporation*, 1982]. The corresponding θ_1 and θ_2 are 5° and 23°, respectively. The maximum slope angle is computed as 19°, which is similar to the current topographic slope angle of 18°. This implies that Hsinshe cumulative fold scarp has a long history and that the "b" segment has been well developed for substantial time.

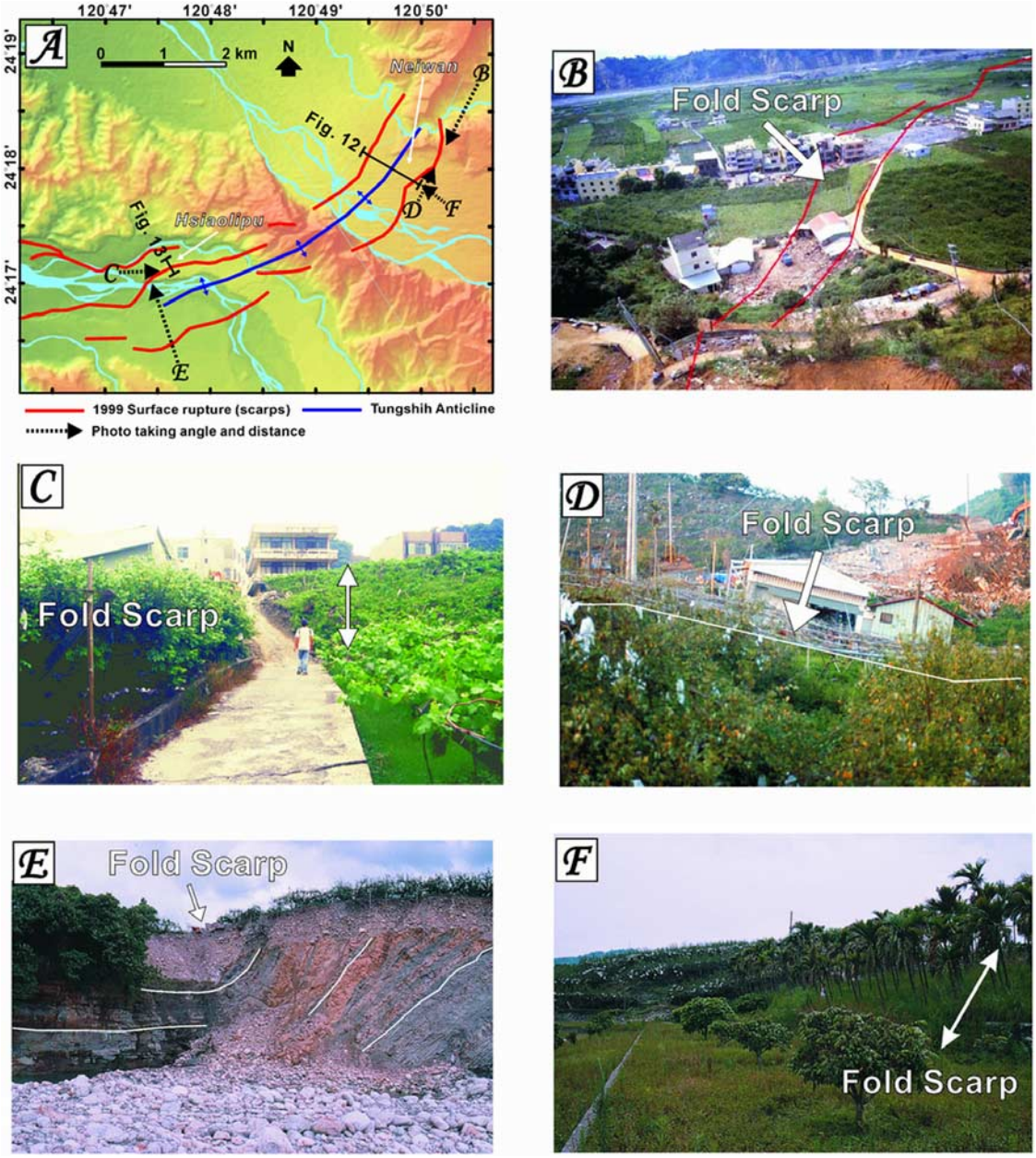

Figure 11. (a) Shaded relief map of the Neiwan and Hsiaolipu areas. The localized 1999 scarps are developed on both limbs of the preexisting Tungshih anticline and face outward. (b) Photo taken from the northern high point shows the southwestern scarp running through the town of Neiwan, where buildings were destroyed above the fold scarp. (c and d) Close-ups of the southeast facing fold scarp which tilted during the 1999 Chi-Chi earthquake. (e) Outcrop along the river bank showing continuous but bent strata underlying the Hsiaolipu fold scarp. The deformed upper terrace is shown in Figure 11f. (f) Hsiaolipu cumulative fold scarp reactivated in 1999.

bend up from 4–8° to 48–55° over a distance of 15 m (Figure 13). On the basis of the dips, a maximum slope angle of 51° can be derived. The current slope angle is measured as only 25°, indicating this terrace is young and has gone through only the early stage of scarp development.

8. Discussion

8.1. Long-Term Evolution of Fold Scarps

[14] Type 1 fold scarps defined in this study begin to form once the fault tip is covered by thick later deposits. The amplification of such scarps will be terminated when the propagating fault tip again reaches the ground surface or when further deposition again buries the fault and the process is renewed. During this developmental history, it is unlikely that there will be a steady growth in scarp amplitude because of the combined effects of episodic deposition and fault tip migration with associated trishear folding. However, the future coseismic deformation still can be predicted to some degree by modeling the deformation in one slip event of the overlying strata and its underlying structural geometry.

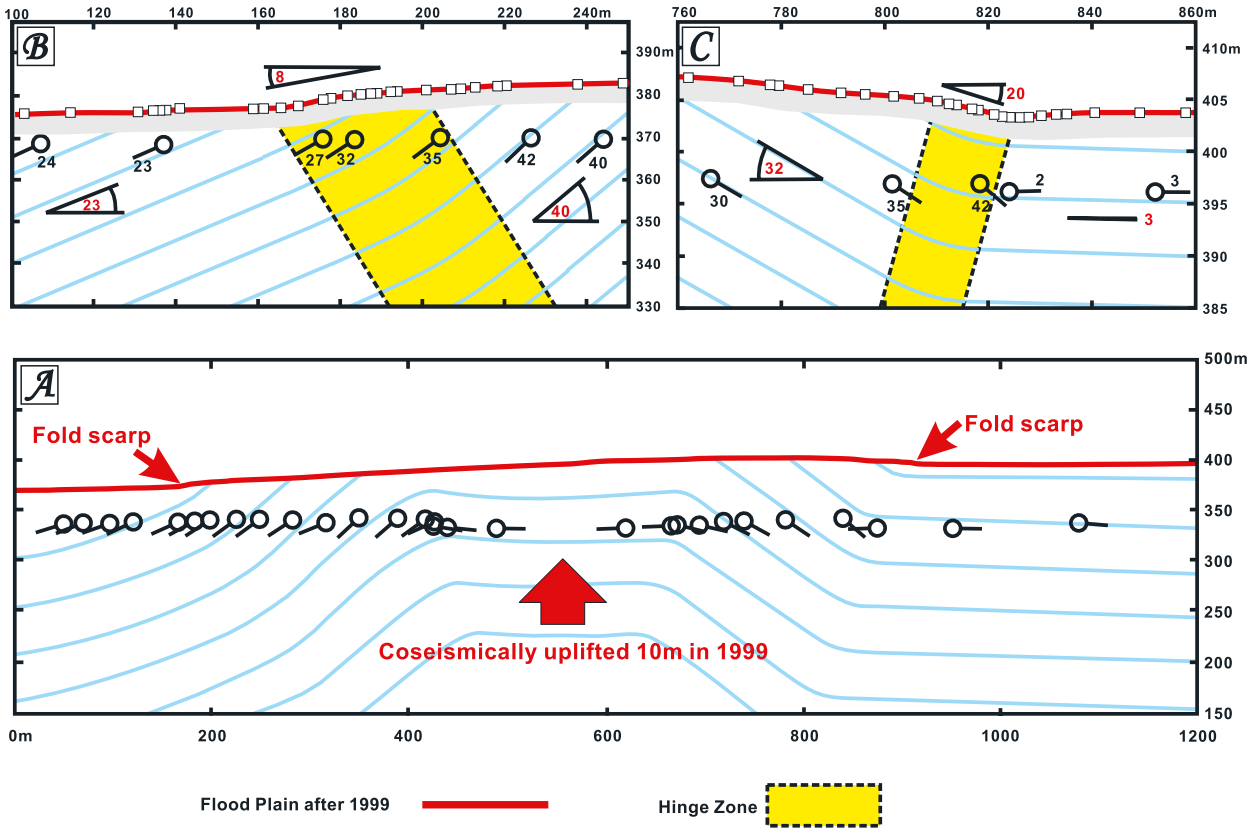

Figure 12. (a) Profile showing the reconstructed subsurface structure and topography across the Tungshih anticline in Neiwan. According to a previous study [*Lee et al.*, 2005], the Tungshih anticline grew by ~10 m and created two rupture scarps located on both of the limbs and facing outward. (b) Close-up profile across the western fold scarp showing a gradual dip change over a horizontal distance of 40 m. A maximum slope angle is computed as 16° by using 23° and 40° as the θ_1 and θ_2, respectively, indicating this scarp needs at least one more event to reach the maximum slope angle. (c) Close-up profile across the eastern fold scarp shows an abrupt dip change in a distance of 8 m. On the basis of the measured dips of 2° and 32°, the maximum scarp angle is 30° which could be reached in future events.

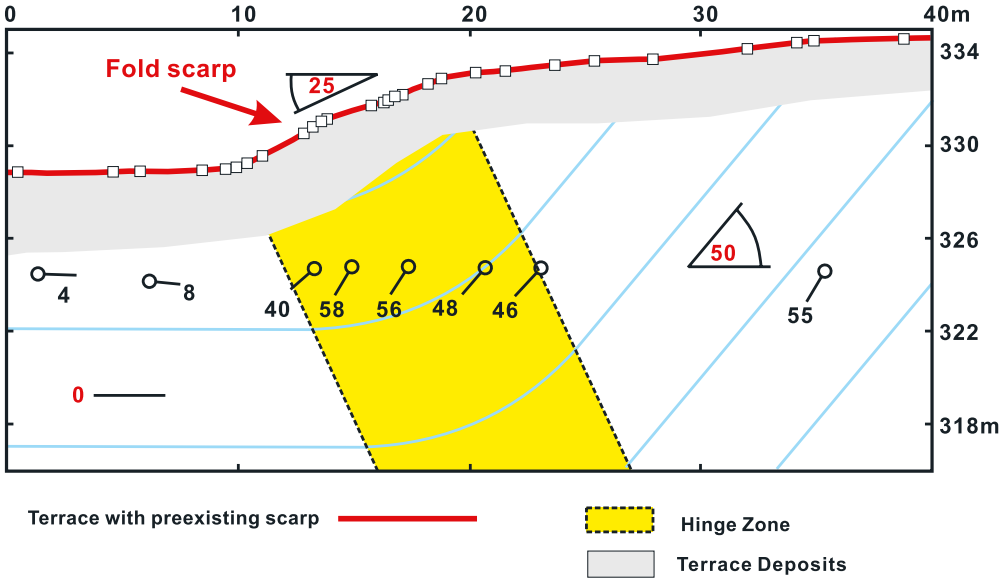

Figure 13. Profiles showing reconstructed subsurface structure at Hsiaolipu and its corresponding fold scarps. Using 0° and 50° as the θ_1 and θ_2, the maximum slope angle will be 50°. Eventhough the scarp is preexisting, future events will be needed to reach the maximum slope.

[15] The type 2 fold scarps will be developed where flat recent sedimentary deposits or human constructions such as roads or leveled fields overlie an abrupt dip change that is the locus of active kink band migration. This abrupt dip change is typically associated with the fault bend beneath. If the fault is active, coseismic slip causes differential vertical displacement due to the dip change. As described above, a complete fold scarp is composed of three segments a, b, and c as shown in Figure 7. However, in the beginning stage when the cumulative slip recorded by the ground surface is still smaller than the arc length of the hinge zone the scarp is actually composed of incomplete segments "a" and "c" (Figures 6 and 7). The "a" and "c" segments actually become complete simultaneously when the cumulative slip reaches the magnitude of the arc length of the hinge zone (Figure 6b). At that time the limb segment "b" begins to form. Thereafter, the widths of "a" and "c" segment will keep constant but the width of segment "b" will grow in further earthquakes. However, the slope angle of the "b" segment is the maximum slope angle for the entire fold scarp and it will be constant. There is no tectonic-related mechanism for terminating the growth of a type 2 fold scarp. Nevertheless, older and higher scarps will be degraded as a result of erosion.

[16] In summary, a simple recognizable geomorphic or man-made surface must form prior to the onset of deformation as an initial condition for recognizable fold scarp formation. The type 1 scarps are usually found associated with the surface trace of the main fault, especially where there is an alluvial fan developed over the original fault scarp. The type 2 scarps are found in the hanging wall above fault bends and can be far from the surface trace of the main fault.

8.2. Paleoseismology Indicator

[17] Fault scarps can be used as paleoseismologic indicators by dividing the scarp height using the characteristic vertical offset per event if we assume the responsible fault behaves characteristically. Since the deformation behavior of the fold scarp is more complicated than of the fault scarp, numerical modeling or trigonometric method may be needed to extract the associated vertical fault offset. For type 1 fold scarps, the scarp shape evolves as the fault tip migrates. If we can retrieve the deformed stratal configuration by trenching or logging, the trishear modeling procedure [*Erslev*, 1991; *Hardy and Ford*, 1997; *Champion et al.*, 2001] could help in reconstruction of the seismic history [*Streig et al.*, 2006]. Similarly, for future earthquake prediction, the fold scarp growth in the next earthquake can be modeled in the same way. For type 2 fold scarps, the slope angle cannot serve of a paleoseismology indicator when the maximum slope angle has been already reached. Before the maximum slope angle is attained, the slope angle still can be an indicator under the condition that we already understand the hinge zone shape and contribution per event. On the other hand, the scarp height would keep growing since the scarp starts to form and be equal to the fault slip times $[\sin(\theta_2) - \sin(\theta_1)]$. The simple trigonometric method presented above can help decipher the paleoseismological history as well as predict future deformation. It is worth noting here that we must be cautious when analyzing the scarp shape because the original scarp shape may be modified due to the later deposition of sediments coming from surface erosion processes, such as soil creeping or down-slope colluvial sediments. This may not be a serious problem for working on a young scarp but becomes more important for old scarps.

8.3. Lateral Variation of the Fold Scarp

[18] Type 1 fold scarps could be laterally variable in shape and amplitude because of the discontinuous distribution of the thickness of the recent sediments. For instance, a small alluvial fan has a limited size. The fold scarp is therefore usually developed within the fan area and turns into a fault scarp again out of the fan area. Type 2 fold scarps will disappear only when the underlying fault bend ends, but lateral variation may exist as a result of changes in θ_1, θ_2, or hinge zone width. In some cases the fault bend will locally generate a secondary fault scarp within the fold scarp, associated with heterogeneity in the near-surface folded material, such as large contrasts in mechanical layer thickness or strength. For example, secondary faults are commonly observed in fold scarps within man-made structures such as concrete (Figure 9c). However, in general, the deformation behavior of the regional ground surface typically is similar to the model presented above. Although the natural system is more complicated than the simple two-dimensional (2-D) kinematic model, further 3-D mechanical simulations are expected to provide more insight into fold scarp behavior in the future.

8.4. Hazard Mitigation and Set-Back Zone

[19] According to the field observation during the 1999 Chi-Chi earthquake and the discussion above, the coseismic surface deformation observed across fold scarps is entirely different from that observed across the fault scarps. The fault scarps actually absorb almost all the deformation produced by the fault action. In the case of thrust faulting there is a characteristic loss of surface area as a result of the hanging wall overlapping the footwall. Therefore it is acceptable to delineate narrow set-back zones across the fault for hazard mitigation. In contrast, across fold scarps the deformation is distributed in a much wider zone and sometimes asymmetrical (Figure 3 and Appendix B). Fold scarps can exceed 100 m in width [e.g., *Hubert-Ferrari et al.*, 2007]. A simple and narrow set-back zone is not enough to serve the purpose of the hazard mitigation. Since the strain patterns are variable for different types or even different locations, each site has to be regarded as a unique case. Before deciding the configuration of the set-back zone for a fold scarp, detailed work including the study of subsurface structure and coseismic deformation simulation has to be carefully done in advance.

9. Conclusion

[20] During the 1999 Chi-Chi earthquake, linear surface scarps consisted not only of fault scarps but also fold scarps. Two types of fold scarps were identified. One is created by near-surface burial of the fault tip and is governed by the shape of the trishear zone. This type 1 fold scarp is closely associated with the main zone of fault scarps. The second type of fold scarp is typically widely separated from the main surface fault trace and is commonly associated with fault bends at depth. The scarp shape of this type is

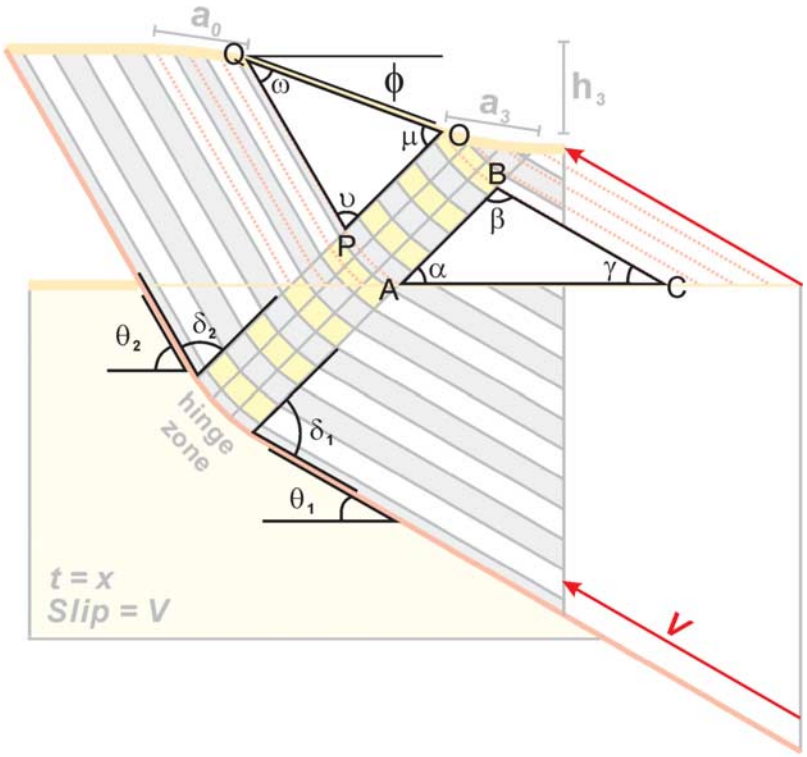

Figure A1. Trigonometric relationships of the slip model of the type 2 fold scarp.

determined by the change in fault dip, the width of the zone of dip change and the total fault slip. The slope of the type 2 fold scarp will grow until a maximum slope angle is reached, which is controlled by the total change in dip of the fault. The scarp height will keep growing at a rate that is proportional to the fault slip rate times the difference in the sines of the fault dip. Both type 1 and type 2 fold scarps can serve as paleoseismic indicators but require a more involved procedure of analysis than commonly used for fault scarps. The wider deformation zone of fold scarps indicates that the set-back zone for hazard mitigation has to be reconsidered for fold scarps.

Appendix A: Maximum Change in Dip Across a Type 2 Fold Scarp

[21] Here we derive a simple relationship for the maximum dip ϕ of a fold scarp caused by displacement of an originally horizontal topographic surface through a fault bend as shown in Figure A1. Bed length and layer thickness are conserved outside the hinge zone and area is conserved within the hinge zone, which is for simplicity modeled as a similar fold of arbitrary shape and finite width. (However, note that this is a special case and not a general solution. However, this is okay for Chelungpu. This is the special case of bedding being parallel to the faults, which is the only case in which slip is conserved across the bend.)

[22] From Figure A1, we have

$$\frac{\sin\alpha}{BC}=\frac{\sin\gamma}{AB}\quad\text{and}\quad\frac{\sin\mu}{PQ}=\frac{\sin\omega}{OP}.$$

Since $V = AP + PQ$, $V = CB + BO$, and $BO = AP$, we obtain $BC = PQ$. Because $AB = OP$, we have

$$\frac{\sin\alpha}{\sin\gamma}=\frac{\sin\mu}{\sin\omega}. \tag{A1}$$

Since the sum of angles of a triangle is 180°, we have $\alpha + \beta + \gamma = 180°$ and $\mu + \nu + \omega = 180°$. Because of the parallel property of the model, we have $\beta + \delta_1 = 180°$, $\gamma = \theta_1$, $\nu = \delta_2$, $\omega = \theta_2 - \phi$, and $\delta_1 = \delta_2 = 90° + \frac{1}{2}(\theta_1 - \theta_2)$. Therefore we can derive $\alpha = 90° - \frac{1}{2}(\theta_1 + \theta_2)$ and $\mu = 90° - \frac{1}{2}(\theta_1 + \theta_2) + \phi$.

[23] Next, we write all variables in terms of θ_1 ,θ_2, and ϕ, then substitute them into equation (1). We obtain

$$\frac{\sin\left[90°-\frac{1}{2}(\theta_1+\theta_2)\right]}{\sin\theta_1}=\frac{\sin\left[90°-\frac{1}{2}(\theta_1+\theta_2)+\phi\right]}{\sin(\theta_2-\phi)}, \tag{A2}$$

which we rewrite using trigonometric identities, as follows:

$$\begin{aligned}
&\frac{\cos\left(\frac{\theta_1+\theta_2}{2}\right)}{\sin\theta_1}=\frac{\cos\left[\frac{\theta_1-\theta_2}{2}+(\theta_2-\phi)\right]}{\sin(\theta_2-\phi)}\\
&\Rightarrow\frac{\cos\left(\frac{\theta_1+\theta_2}{2}\right)}{\sin\theta_1}=\frac{\cos\frac{\theta_1-\theta_2}{2}\cos(\theta_2-\phi)-\sin\frac{\theta_1-\theta_2}{2}\sin(\theta_2-\phi)}{\sin(\theta_2-\phi)}\\
&\Rightarrow\frac{\cos\left(\frac{\theta_1+\theta_2}{2}\right)}{\sin\theta_1}=\cos\frac{\theta_1-\theta_2}{2}\cot(\theta_2-\phi)-\sin\frac{\theta_1-\theta_2}{2}\\
&\Rightarrow\frac{\cos\frac{\theta_1+\theta_2}{2}+\sin\theta_1\sin\frac{\theta_1-\theta_2}{2}}{\sin\theta_1}=\cos\frac{\theta_1-\theta_2}{2}\cot(\theta_2-\phi).
\end{aligned}$$

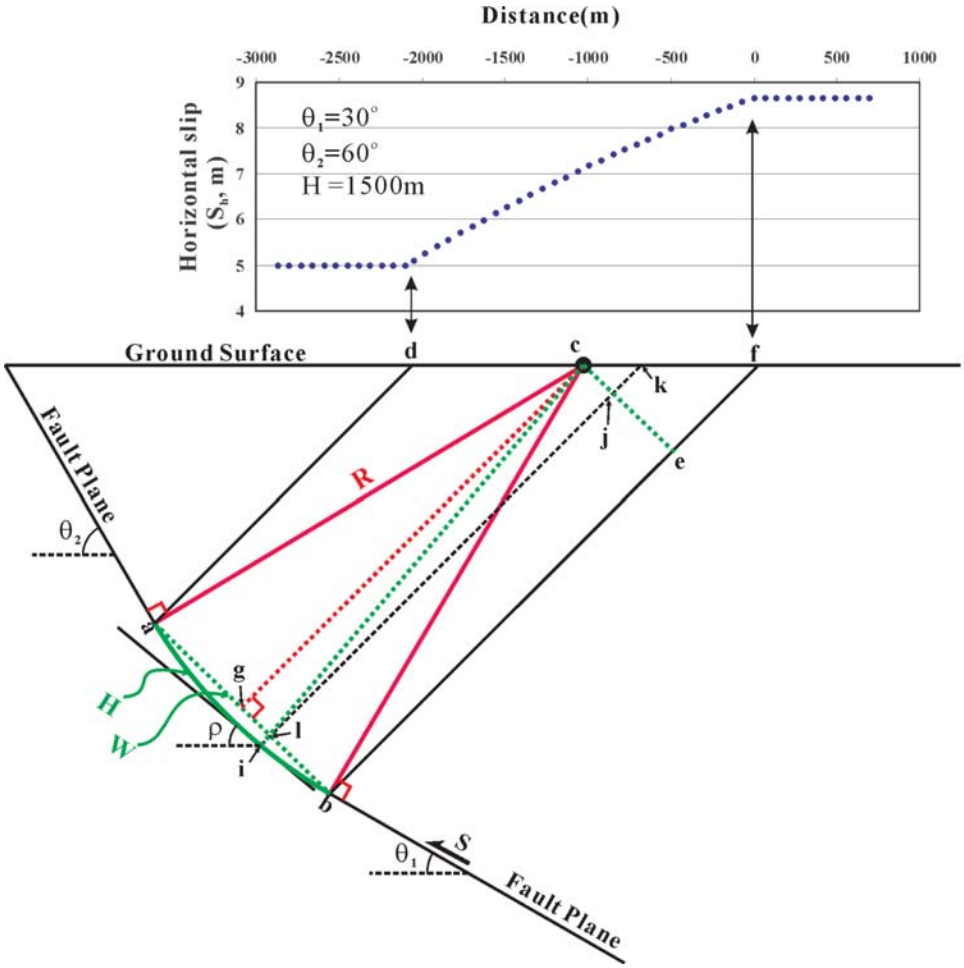

Figure B1. Lower profile showing the geometry of a thrust fault with a curved bend of finite width that can be described by a hinge zone. The upper profile shows the horizontal component of the slip at the ground surface across the projected area of the hinge zone. The values of θ_1, θ_2, the event slip (S), and the hinge zone arc length (H) are assigned as 30°, 60°, 10 m, and 1500 m, respectively. Please also see text for the details.

After solving for cot $(\theta_2 - \phi)$, we rewrite it to tan $(\theta_2 - \phi)$ as follows:

$$\tan(\theta_2 - \phi) = \frac{\sin\theta_1 \cos\frac{\theta_1-\theta_2}{2}}{\cos\frac{\theta_1+\theta_2}{2} + \sin\theta_1 \sin\frac{\theta_1-\theta_2}{2}} = \frac{\sin\theta_1 \cos\frac{\theta_2-\theta_1}{2}}{\cos\frac{\theta_1+\theta_2}{2} - \sin\theta_1 \sin\frac{\theta_2-\theta_1}{2}}.$$

Appendix B: Velocity Field Across the Type 2 Fold Scarp

[24] We derive a simple velocity field associated with a type 2 fold scarp, assuming a similar fold geometry and conservation of slip through the fault bend, implying a transient dilatancy within the hinge zone but no net dilatancy, which is acceptable because we do not wish to model poorly understood hinge zone processes. For simplicity, we assume a hinge shape composed of a circular arc, but the results are not highly sensitive to any choice of geologically reasonable hinge for sedimentary strata shapes that are wide relative to mechanical layer thickness. All particles are assumed to move parallel to the fault, which is consistent with a bedding-parallel fault in the hanging wall.

[25] We assume a thrust fault bends upward from a dip of θ_1 to a dip of θ_2 with a hinge zone of finite width extending from point "b" to "a" (Figure B1). The hinge width (W) normal to the bisecting axial surface is the line segment from "a" to "b". The fault plane within the hinge zone is assumed to be a circular arc segment (H) of "a" to "b" with a center of curvature at point "c" and a radius R. An applied slip on the fault plane "S" happens along the fault plane has a horizontal component (Sh) that is simply S*cos(fault dip). For all points prior to entry into the hinge zone, Sh = S*cos(θ_1), whereas for all points that have moved beyond the hinge zone, Sh = S*cos(θ_2).

[26] Along the arc (H) the fault dips change from θ_1 to θ_2. For each point along the arc the dip is equal to the included angle (ρ) of the tangent and horizontal line. The horizontal component of slip Sh is cos(ρ) and by the similar fold assumption is identical along the line from i to k. Similar relationships hold for the vertical component; therefore the simple velocity field is everywhere defined.

[27] On the basis of Figure B1, the ρ angle can be expressed as

$$\angle dca = 90^\circ - \theta_2, \angle dca + \angle acb = 90^\circ - \theta_1$$
$$\therefore \angle acb = \theta_2 - \theta_1 \qquad \angle acg = \frac{\theta_2 - \theta_1}{2}$$
$$\angle fce = 180^\circ - 90^\circ - \angle acb - \angle acg = \frac{\theta_2 + \theta_1}{2}$$

From former equation, we can know

$$\widehat{H} = \frac{\angle acb \times \pi \times R}{180^\circ}$$
$$\widehat{H} = \frac{(\theta_2 - \theta_1) \times \pi \times R}{180^\circ}$$
$$\therefore R = \frac{180^\circ \times \widehat{H}}{(\theta_2 - \theta_1) \times \pi}$$
$$W = 2 \times \sin(\angle acg) \times R$$
$$W = 2 \times \sin\left(\frac{\theta_2 - \theta_1}{2}\right) \times R$$
$$\overline{bg} = \frac{W}{2} = \sin\left(\frac{\theta_2 - \theta_1}{2}\right) \times R$$
$$\angle lcb = \rho - \theta_1$$
$$\overline{gl} = \sin\left(\frac{\theta_2 - \theta_1}{2} - (\rho - \theta_1)\right) \times R$$
$$\overline{bl} = \overline{bg} - \overline{gl}$$
$$\therefore \overline{bl} = \sin\left(\frac{\theta_2 - \theta_1}{2}\right) \times R - \sin\left(\frac{\theta_2 - \theta_1}{2} - (\rho - \theta_1)\right) \times R = \overline{ej}$$
$$\rho = \frac{\theta_2 + \theta_1}{2} - \sin^{-1}\left(\sin\left(\frac{\theta_2 - \theta_1}{2}\right) - \frac{\overline{bl}}{R}\right)$$

if we let l be a point moving from b to a, then define x = bl such that x varies from 0 to W,

then

$$\rho = \frac{\theta_2 + \theta_1}{2} - \sin^{-1}\left(\sin\left(\frac{\theta_2 - \theta_1}{2}\right) - \frac{x}{R}\right)$$

[28] **Acknowledgments.** This study is financially supported by National Science Council of Taiwan under grants NSC92-2116-M-002 and 93-2119-M-002-026. We thank the Editors and reviewers, John Mutter, Jean-Philippe Avouac, Richard Walker, and another anonymous for their helpful suggestions and comments. We are also grateful for the strong support of the field work from the Central Geological Survey of Taiwan.

References

Bonilla, M. G. (1977), Summary of quaternary faulting and elevation changes in Taiwan, *Mem. Geol. Soc. China*, *2*, 43–55.

Central Geological Survey (CGS) (1999), Investigation report of 921 earthquake geology and map of surface ruptures along the Chelungpu Fault during the 1999 Chi-Chi earthquake (in Chinese), Minist. of Econ. Affairs, Taipei, Taiwan.

Champion, J., K. Mueller, A. Tate, and M. Guccione (2001), Geometry, numerical models and revised slip rate for the Reelfoot fault and trishear fault-propagation fold, New Madrid seismic zone, *Eng. Geol.*, *62*, 31–49.

Chen, W. S., K. J. Lee, L. S. Lee, D. J. Ponti, C. Prentice, Y. G. Chen, H. C. Chang, and Y. H. Lee (2004), Paleoseismology of the Chelungpu Fault during the past 1900 years, *Quat. Int.*, *115/116*, 167–176.

Chen, Y. G., W. S. Chen, Y. Wang, P. W. Lo, J. C. Lee, and T. K. Liu (2002), Geomorphic evidence for prior earthquakes: Lessons from the 1999 Chichi earthquake in central Taiwan, *Geology*, *30*(2), 171–174.

Chinese Petroleum Company (1982), The geological map of Taichung, Taiwan, scale 1:100000, Taiwan Pet. Explor. Div., Taipei.

Chiu, H. T. (1971), Fold in the northern half of western Taiwan, *Petrol. Geol. Taiwan*, *8*, 7–19.

Dolan, J. F., S. Christofferson, and J. H. Shaw (2003), Recognition of paleoearthquakes on the Puente Hills blind thrust fault, Los Angeles, California, *Science*, *300*, 115–118.

Erslev, E. A. (1991), Trishear fault-propagation folding, *Geology*, *19*, 617–620.

Hardy, S., and M. Ford (1997), Numerical modeling of trishear fault propagation folding, *Tectonics*, *16*, 841–854.

Ho, C. S. (1982), *Tectonic Evolution of Taiwan—Explanatory Text of the Geologic Map of Taiwan*, 126 pp., Central Geol. Surv., Minist. of Econ. Affairs, Taipei, Taiwan.

Hu, C. C., and H. T. Chiu (1984), Deep structures of the Cholan Area, northern Taiwan, *Petrol. Geol. Taiwan*, *20*, 21–33.

Hubert-Ferrari, A., J. Suppe, R. Gonzalez-Mieres, and X. Wang (2007), Mechanisms of active folding of the landscape (southern Tian Shan, China), *J. Geophys. Res.*, doi:10.1029/2006JB004362, in press.

Kao, H., and W. P. Chen (2000), The Chi-Chi earthquake sequence: Active, out-of-sequence thrust faulting in Taiwan, *Science*, *288*, 2346–2349.

Ku, C. C. (1963), Photogeologic study of terraces in north-western Taiwan, *Proc. Geol. Soc. China*, *6*, 51–60.

Lai, K. Y., Y. G. Chen, J. H. Hung, J. Suppe, L. F. Yue, and Y. W. Chen (2006), Surface deformation related to kink-folding above an active fault: Evidence from geomorphic features and co-seismic slips, *Quat. Int.*, *147*, 44–54.

Lee, Y. H., S. T. Lu, T. S. Shih, M. L. Hsieh, and W. Y. Wu (2005), Structures associated with the northward ending of the 1999 Chi-Chi earthquake rupture, central Taiwan, and their implications on seismic hazard assessment, *Bull. Seismol. Soc. Am.*, *95*(2), 471–485.

Ma, K. F., C. T. Lee, Y. B. Tsai, T.-C. Shin, and J. Mori (1999), The Chi-Chi, Taiwan earthquake: Large surface displacements on an inland thrust fault, *Eos Trans. AGU*, *80*, 605.

Shih, T. T., J. C. Chang, K. S. Yang, and M. Y. Hsu (1985), Active faults and geomorphic surfaces of the Tsaotun and Chelungpu terraces (in Chinese), *J. Geogr. Sci.*, *13*, 1–12.

Shih, T. T., K. S. Teng, K. S. Yang, and M. Y. Hsu (1986), Active faults and geomorphic surfaces of the Hsinshe terraces (in Chinese), *Geomorph. Bull.*, *5*, 29–39.

Streig, A., C. M. Rubin, W. S. Chen, Y. G. Chen, L. S. Lee, S. T. Lu, S. Thompson, and S. Y. Huang (2006), Evidence for prehistoric coseismic folding along the Tsaotun segment of the Chelungpu fault near Nan-Tou, Taiwan, *J. Geophys. Res.*, doi:10.1029/2006JB004493, in press.

Suppe, J. (1981), Mechanics of mountain building in Taiwan, *Mem. Geol. Soc. China*, *4*, 67–89.

Suppe, J. (1986), Reactivated normal faults in the western Taiwan fold and-thrust belt, *Mem. Geol. Soc. China*, *7*, 187–200.

Suppe, J., F. Sabat, J. A. Muños, J. Poblet, E. Roca, and J. Verges (1997), Bed-by-bed fold growth by kink-band migration: Sant Llorenç de Morunys, eastern Pyrenees, *J. Struc. Geol.*, *19*, 443–461.

Teng, L. S. (1990), Geotectonic evolution of late Cenozoic arc-continent collision in Taiwan, *Tectonophysics*, *183*, 57–76.

Yielding, G., J. A. Jackson, G. King, H. Sinvhal, C. Vita-Finzi, and R. Wood (1981), Relations between surface deformation, fault geometry, seismicity and rupture characteristics during the El Asnam (Algeria) earthquake of 10 October 1980, *Earth Planet. Sci. Lett.*, *56*, 287–304.

Yu, S. B., L. C. Kuo, R. S. Punongbayan, and E. G. Ramos (1999), GPS observation of crustal deformation in the Taiwan-Luzon region, *Geophys. Res. Lett.*, *26*(7), 923–926.

Yue, L. F., J. Suppe, and J. H. Hung (2005), Structural geology of a classic thrust belt earthquake: The 1999 Chi-Chi earthquake Taiwan (M_w = 7. 6), *J. Struct. Geol.*, *27*, 2058–2083.

W.-S. Chen, Y.-G. Chen, Y.-T. Kuo, K.-Y. Lai, Y.-N. N. Lin, and Y. Wang, Department of Geosciences, National Taiwan University, P.O. Box 13-318, Taipei 106, Taiwan. (ygchen@ntu.edu.tw)

J.-H. Hung, Department of Earth Sciences, National Central University, Chungli 320, Taiwan.

Y.-H. Lee, Department of Earth and Environmental Sciences, National Chung-Cheng University, Chiayi 621, Taiwan.

J. Suppe, Department of Geosciences, Princeton University, Princeton, NJ 08544, USA.